Top Catal (2009) 52:470–481
DOI 10.1007/s11244-009-9187-3

ORIGINAL PAPER

Synthesis and Characterization of Manganese Oxide Catalysts for the Total Oxidation of Ethyl Acetate

V. P. Santos · M. F. R. Pereira · J. J. M. Órfão · J. L. Figueiredo

Published online: 24 February 2009

Abstract Manganese oxide catalysts were synthesized by direct reaction between manganese acetate and permanganate ions, under acidic and reflux conditions. Parameters such as pH (2.0–4.5) and template cation (Na^+, K^+ and Cs^+) were studied. A pure cryptomelane-type manganese oxide was synthesized under specific conditions, and it was found that the template cation plays an important role on the formation of this kind of structure. Cryptomelane was found to be a very active oxidation catalyst, converting ethyl acetate into CO_2 at low temperatures (220 °C). This catalyst is very stable at least during 90 h of reaction and its performance is not significantly affected by the presence of water vapour or CO_2 in the feed stream. The catalyst performance can be improved by the presence of small amounts of Mn_3O_4.

Keywords Manganese oxides · OMS · Cryptomelane · Oxidation · VOC · Ethyl acetate

V. P. Santos · M. F. R. Pereira · J. J. M. Órfão · J. L. Figueiredo (✉)
Laboratório de Catálise e Materiais (LCM), Laboratório Associado LSRE/LCM, Departamento de Engenharia Química, Faculdade de Engenharia, Universidade do Porto, Rua Dr. Roberto Frias, Porto 4200-465, Portugal
e-mail: jlfig@fe.up.pt

V. P. Santos
e-mail: santos.vera@fe.up.pt

M. F. R. Pereira
e-mail: fpereira@fe.up.pt

J. J. M. Órfão
e-mail: jjmo@fe.up.pt

1 Introduction

In the past decade, manganese oxides have been intensively investigated due to their high economic value and potential applications in heterogeneous catalysis, in particular for oxidation processes [1–3]. Extensive research efforts have been devoted to the synthesis of this kind of material, the so called octahedral molecular sieves (OMS) with layer and tunnel structures [4–10]. The open frameworks of these materials are composed of edge and corner shared MnO_6 octahedra, the internal pores being occupied by cations and water molecules. Cryptomelane-type manganese oxide (K-OMS-2) is one group of the OMS family called hollandite, and has tunnel structures that consist of 2 × 2 arrays of MnO_6 octahedra [7, 11, 12]. Inside the tunnels, potassium cations and small amounts of water stabilize the structure, and can be partially ion-exchanged with other cations with appropriate sizes. The tunnel size is 0.46 nm × 0.46 nm and the average manganese oxidation state is around 3.8, which reflects a vast majority of Mn(IV) with lower amounts of Mn(III). The open tunnel structure and mixed valences of OMS-2 make this material very attractive for oxidation catalysis and, therefore, the synthesis of OMS-2 material with high purities, small particle size, high surface areas, and high yield has been a challenge in recent years. Various synthetic routes have been explored [13], including thermal and hydrothermal treatment of layered birnessite [14], redox precipitation under reflux [7, 15], microwave heating [16], sol-gel methods [17, 18] and a solvent free procedure [19]. The reflux method, involving the oxidation of Mn^{2+} by MnO_4^-, is the most common route. Reaction parameters, such as temperature, pH, concentration of reactants and template cation, are believed to bear a critical impact on the formation of cryptomelane. In spite of the intensive research that has been carried out in

this area, the effect of these parameters on the crystallinity, stability and morphologies of OMS-2 material is not yet completely clear.

In this report we use the reflux approach to produce cryptomelane-type manganese oxides, by a direct reaction between manganese acetate and permanganate ions under acidic and reflux conditions. Parameters such as pH and template cation were studied. It is well known that during hydrothermal transformation, cations will stay in the tunnels to stabilize and support the tunnel structures. Therefore, it is expected that the template cation (such as cesium or sodium, alone or mixed with potassium), will have an important effect on the cryptomelane structure obtained. The shapes, crystal forms, average oxidation states and stabilities of these materials were evaluated. The catalytic performance of all materials was tested in the ethyl acetate oxidation.

2 Experimental

2.1 Synthesis

Manganese oxides were synthesized by the reflux method developed by Luo et al. [15]. 11 g of $Mn(CH_3COO)_2 \cdot 4H_2O$ (Fluka, 99% purity) were dissolved in 40 mL of water. The pH of this solution was maintained using a buffer solution (KCH_3COO/CH_3COOH, Fluka, 99% purity) or concentrated nitric acid (Panreac, 65%), in order to ensure different pH values (Table 1). A Total of 6.5 g of $KMnO_4$ (Vaz Pereira, 99% purity) were dissolved in 150 mL of water, and this solution was slowly added to the previous one. The black precipitate formed was stirred and refluxed at 100 °C for 24 h. The solid obtained was filtered and washed with distilled water, dried in an oven and calcined at 450 °C in air for 4.5 h. To study the effect of the template cation on the products obtained, two procedures were used: in the first one $NaMnO_4$ or $CsMnO_4$ were used in the presence of the buffer solution and in the second nitric acid was used to control the pH (pH 4.5), as summarized in Table 1.

Table 1 Synthesis parameters of the prepared oxides

Sample	Oxidant agent	pH control	Initial pH
Mn1	$KMnO_4$	CH_3COOH/KCH_3COO	4.5
Mn2	$KMnO_4$	HNO_3	3.5
Mn3	$KMnO_4$	HNO_3	3
Mn4	$KMnO_4$	HNO_3	2
Mn5	$NaMnO_4$	CH_3COOH/KCH_3COO	4.5
Mn6	$CsMnO_4$	CH_3COOH/KCH_3COO	4.5
Mn7	$NaMnO_4$	HNO_3	4.5
Mn8	$CsMnO_4$	HNO_3	4.5

2.2 Characterization

All samples were characterized by X-ray diffraction (XRD), X-ray photoelectron spectroscopy (XPS), scanning electron microscopy/energy dispersive X-ray spectroscopy (SEM/EDS), N_2 adsorption at 77 K, thermogravimetric analysis (TGA) and temperature programmed desorption (TPD).

2.2.1 Structure and Morphology

The structure and phase purity of the prepared materials were analysed by X-ray diffraction using a PANalytical X'Pert PRO diffractometer with Cu K_α radiation source ($\lambda = 0.154$ nm) and with a beam voltage of 50 kV and 40 mA of beam current. The data were collected in the 2θ range of 10°–100° with a scanning rate of 0.017°/s. The morphology of the materials was studied by field emission scanning electron microscopy (FEG-ESEM) on a FEI Quanta 400FEG/EDAX Genesis X4M with a Schottky Emitter at an accelerating voltage of 10 kV.

2.2.2 Average Oxidation State

The average oxidation state of manganese in all materials was obtained by XPS. XPS analysis was performed with a VG Scientific ESCALAB 200A spectrometer using Al K_α radiation (1486.6 eV). Charging effects were corrected by adjusting the binding energy of C 1s to 284.6 eV.

2.2.3 N_2 Adsorption at 77 K

Nitrogen adsorption isotherms were obtained with a Quantachrome Instruments Nova 4200e. The samples were pre-degassed at 300 °C for 3 h. Nitrogen was used as adsorbate at liquid nitrogen temperature.

2.2.4 Thermal Stability

Thermogravimetric analysis (TGA) was done on a Mettler TA 4000 system under air or nitrogen atmospheres. About 10 mg of sample were loaded into a ceramic sample holder and the temperature was raised to 900 °C at 10 °C/min. Thermal stability of the materials was also studied by temperature programmed desorption combined with a mass spectrometer (TPD-MS). These experiments were conducted on an Altamira Instruments (AMI 200) apparatus. A total of 100 mg of the sample was loaded in the reactor and placed inside the furnace. The sample was purged with helium for 1 h at room temperature followed by heating to 900 °C at 5 °C/min in the same atmosphere.

2.3 Catalytic Activity Measurements

The catalytic oxidation of ethyl acetate was performed under atmospheric pressure in a fixed-bed reactor from Autoclave Engineers (BTRS Jr), which consists of a stainless steel tube of 6 mm internal diameter, placed inside a PID controlled electric furnace. Temperature in the reaction zone was measured by a K type thermocouple placed in the middle of the catalyst bed. In order to minimize the thermal effects, the catalyst bed was diluted with glass spheres of the same size as the catalyst particles ($0.2 < \varphi < 0.5$ mm). Prior to the reaction the catalyst was activated under air at 400 °C for 1 h. A feed gas with 1,600 ppmv of ethyl acetate and a space velocity of 16,000 h^{-1} was used in the standard conditions. The space velocity quoted was defined in terms of the total bed volume (catalyst + inert).

The reaction temperature was raised from 160 to 260 °C by steps of 10 °C. The reactor was maintained at each temperature for 30 min in order to obtain experimental values at steady state. The ethyl acetate conversion (X) and the conversion into CO_2 (X_{CO_2}) were respectively calculated as $X = 1 - \frac{F_{VOC}}{F_{VOC,in}}$ and $X_{CO_2} = \frac{F_{VOC}}{vF_{VOC,in}}$ where F_{VOC} is the outlet molar flow rate of VOC at steady state, $F_{VOC,in}$ is the inlet molar flow rate of VOC, F_{CO_2} is the outlet molar flow rate of CO_2 at steady state and v is the number of carbon atoms in the VOC molecule (for ethyl acetate, $v = 4$).

The analytical system consisted of a gas chromatograph equipped with a flame ionization detector (FID) for the analysis of the organic compounds, and an online non-dispersive infrared (NDIR) analyzer for CO_2 detection and quantification.

3 Results and Discussion

3.1 Characterization

3.1.1 Structure and Morphology

Cryptomelane is synthesized by the reaction between Mn^{2+} and MnO_4^- in acid medium, in which an amorphous phase of manganese oxide is formed according to the equation $2MnO_4^- + 3Mn^{2+} + 2H_2O \rightarrow 5MnO_2 + 4H^+$; subsequently, the mixture is maintained in reflux during 24 h at 100 °C to obtain the nanostructured oxide.

This synthesis mainly depends on three factors: temperature, pH and the template cation. In order to understand the effect of pH and template cation on OMS-2 formation, three types of procedures were used (Table 1). In the first one, $KMnO_4$ was used as oxidant, and the initial pH was adjusted at 3.5, 3.0 and 2.0 using nitric acid, and 4.5 using a buffer solution of KCH_3COO/CH_3COOH. In the second and third procedures, $NaMnO_4$ or $CsMnO_4$ were used as oxidants, and the pH was adjusted by using the same buffer solution, or nitric acid, respectively (in the last case, there was no source of potassium).

XRD allowed to study the effect of pH and template cation on the crystallization process of OMS-2 (Fig. 1). Figure 1a shows the XRD patterns for all materials prepared with $KMnO_4$. All positions of the diffractions lines in the XRD patterns of OMS-2 materials produced at pH 4.5, 3.5 and 3.0 are in good agreement with the standard pattern of the pure tetragonal cryptomelane Q-phase with lattice parameters $a = b = 0.9917$ nm and $c = 0.22738$ nm (KMn_8O_{16}, JCPDS 42-1348), although the relative intensities do not exactly match the theoretical data. This fact may result from defects in the lattice (primarily O defects), small crystal size, preferential ordering (anisotropic crystallite morphology) or different quantities of potassium cations [6]. At the lowest pH, α-Mn_2O_3 was detected as impurity. Additionally, it may be observed that the widths of the peaks of OMS-2 materials produced with nitric acid are larger than those produced with the buffer solution, which indicates small crystallite sizes. The calculation of the crystallite sizes from Scherrer's equation at $2\theta = 37.5°$ and $2\theta = 28.7°$ suggest a range between 30 and 16 nm.

Figure 1b and c show the effect of the template cation on the structure of manganese oxide materials. When $KMnO_4$ was replaced by $NaMnO_4$ or $CsMnO_4$, using the buffer solution to control the pH (source of potassium cations in the medium), no pure cryptomelane phase was observed. In the first case (Mn5), small amounts of Mn_3O_4 were detected, while in the second case (Mn6) a more complex spectrum was obtained: α-Mn_2O_3 was identified as the major impurity and residual amounts of Mn_5O_8 might be present.When potassium cations were completely removed from the reactant mixture (Fig. 1c), no cryptomelane structure was attained, but instead a mixture of α-Mn_2O_3 and β-MnO_2 (small amounts). This result shows that potassium cations in the reactant medium play an important role for the formation of the tunnel structure and the incorporation of monovalent cations such as Na^+ and Cs^+ in the manganese structure was unsuccessful. Table 2 summarises these results.

Figure 2 shows SEM micrographs of the prepared materials. Fibers or needle-like particles, typical of cryptomelane [11, 20], are observed in samples synthesized under different pH with $KMnO_4$ (samples Mn1 to Mn4). In all cases considered, the nanofibers have very long lengths that vary from a few hundred nanometers to a few micrometers, and widths in the middle varying from 10 to 30 nm, characteristic of the method used [19]. However, it seems that the materials prepared with nitric acid have small fiber widths compared to those prepared with the buffer

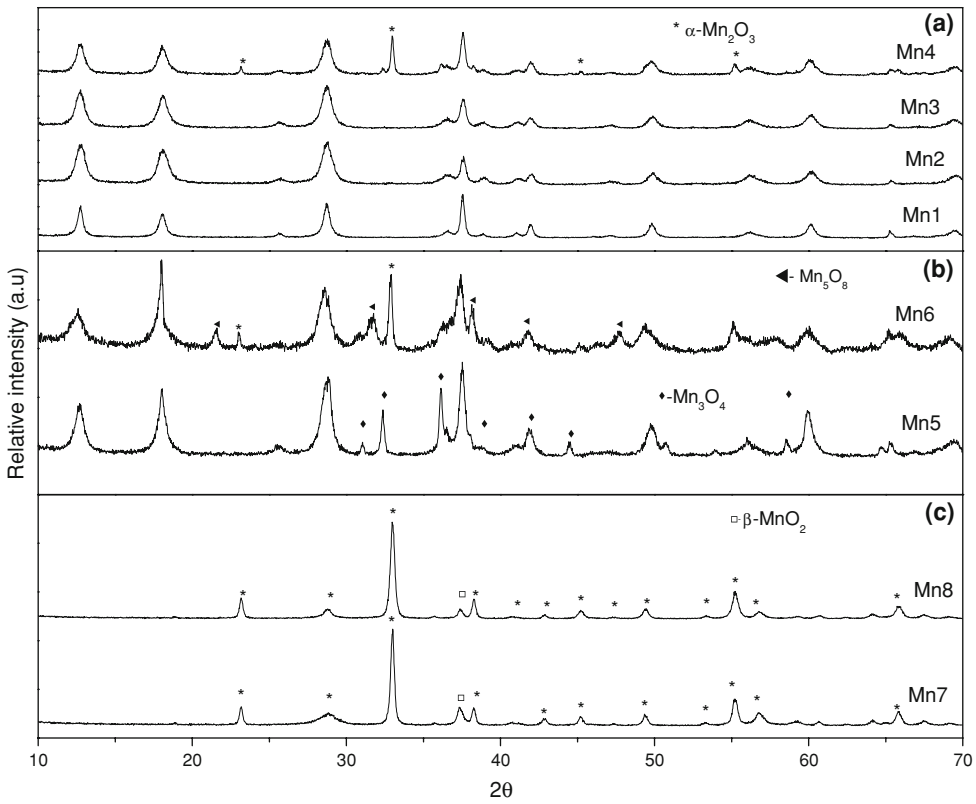

Fig. 1 XRD spectra of the synthesized materials: (a) Mn1–Mn4, (b) Mn5–Mn6, (c) Mn7–Mn8. The samples are identified in Table 1

Table 2 Manganese oxides detected by XRD in the prepared samples

Sample	pH	Dopant cation	K/Mn	X/Mn	Product
Mn1	4.5	K^+	2:1	–	KMn_8O_{16}
Mn2	3.5	K^+	1:1	–	KMn_8O_{16}
Mn3	3.0	K^+	1:1	–	KMn_8O_{16}
Mn4	2.0	K^+	1:1	–	KMn_8O_{16}; α-Mn_2O_3
Mn5	4.5	K^+, Na^+	1.1:1	0.91:1	KMn_8O_{16}; Mn_3O_4
Mn6	4.5	K^+, Cs^+	1.1:1	0.91:1	KMn_8O_{16}, α-Mn_2O_3, (Mn_5O_8)
Mn7	4.5	Na^+	–	0.91:1	α-Mn_2O_3, β-MnO_2
Mn8	4.5	Cs^+	–	0.91:1	α-Mn_2O_3, β-MnO_2

solution, which is consistent with the XRD results. EDS analysis confirms the presence of K, Mn and O and there is a gradual decrease in the K/Mn ratio as the pH decreases, except for the lowest pH as can be seen in Table 3. The atomic ratios of potassium to manganese cations on the surface are relatively lower than the ideal ratio of K/Mn (0.25) in cryptomelane [11], which may indicate the presence of more vacancies in octahedral sites of manganese.

Figure 2e shows that the replacement of $KMnO_4$ for $NaMnO_4$ does not promote a significant change in morphology, while the use of $CsMnO_4$ creates two different microstructures (Fig. 2f): the first one corresponds to cryptomelane with the typical nanofibrous appearance and the second is MnO_x which has a quadrangular prism shape. In order to confirm the composition of the two single phases, EDS experiments were performed in zones identified by Z1 and Z2 (Fig. 2f, inset). Z2 contains only Mn and O, while the Z1 zone contains K, Mn and O, which supports the presence of MnO_x and cryptomelane, respectively.

Figure 2g and h show that a MnO_x structure was formed in the absence of potassium cations, with a shape that depends on the kind of template cation present. When $CsMnO_4$ was used, a typical sheetlike morphology and, to a lower extent, thin fibers, were obtained. Similar morphologies were reported when refluxing the aqueous solution containing $Mn(ClO_4)_2$, $(C_2H_5)_4NOH$, and $CsMnO_4$ at 100 °C for 11 days [21]. In the case of $NaMnO_4$, irregularly shaped globules and thin fibers were obtained. The presence of Mn and O was confirmed by EDS analysis in both samples.

3.1.2 Manganese Valency

The average oxidation state of manganese (AOS) in all samples was obtained by XPS. Table 3 displays the binding energies of Mn $2p_{1/2}$ and Mn $2p_{3/2}$. As can be seen, those values do not change significantly. It is well known that Mn(II), Mn(III) and Mn(IV) have essentially the same binding energy in the perovskite sample, so it is difficult to identify the oxidation state only by the binding energy shift

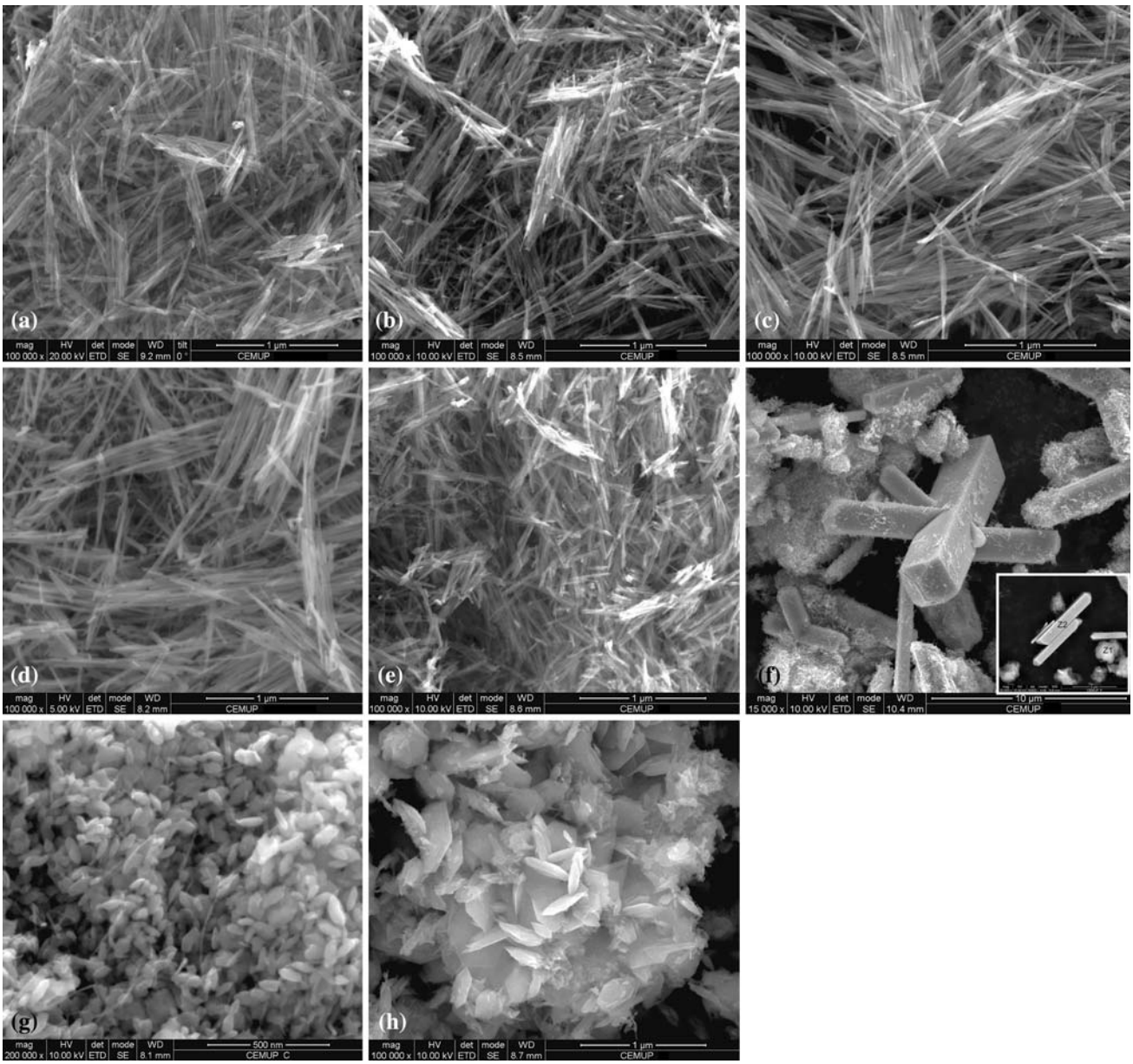

Fig. 2 FESEM images of the materials: **a** Mn1, **b** Mn2, **c** Mn3, **d** Mn4, **e** Mn5 **f** Mn6 **g** Mn7, **h** Mn8

Table 3 Catalyst characterization by XPS, EDS and nitrogen adsorption

Sample	E [Mn 2p] (eV)		ΔE_s[Mn 3s] (eV)	AOS	K/Mn (atomic ratio)		S_{BET} (m^2/g)
	$2p_{1/2}$	$2p_{3/2}$			Bulk	Surface	
Mn1	642.2	653.8	4.50	+3.89	0.13	0.21	45
Mn2	642.3	653.9	4.50	+3.89	0.11	0.17	71
Mn3	642.2	653.9	4.56	+3.82	0.09	0.14	65
Mn4	642.3	653.9	4.63	+3.74	0.11	0.17	45
Mn5	642.1	653.9	4.65	+3.72	0.14	0.23	84
Mn6	642.1	653.8	4.63	+3.74	0.10	0.14	59
Mn7	642.0	653.6	4.60	+3.78	0	0	46
Mn8	641.9	653.6	4.64	+3.73	0	0	25

of Mn 2p [22]. Galakhov et al. [23] proposed that the XPS of Mn 3s is more promising for identifying the manganese oxidation state. Mn 3s exhibits an exchange splitting in its X-ray photoelectron spectrum, promoted by the exchange coupling between the 3s holes and the 3d electrons [23, 24]. The magnitude of the 3s splitting is proportional to $(2S + 1)$ where S is the value of the local spin of the 3d electrons in the ground state. Since the splitting depends on the d configuration, the manganese valency can be estimated.

According to this and to the relationship between ΔEs and the average oxidation state (AOS) reported by Galakhov et al. [23], the AOS of all materials were calculated using the formula $\text{AOS} = 8.956 - 1.126\ \Delta E_s(\text{eV})$.

Table 3 shows that all cryptomelane materials prepared at pH 4.5, 3.5 and 3.0 have an AOS between 3.8 and 3.9, which is in agreement with the mixed state of manganese in the framework of cryptomelane (coexistence of Mn(IV) and a minor amount of Mn(III)) [6, 19]. The AOS of cryptomelane obtained at pH 2.0 is lower, due to the presence of the α-Mn_2O_3 phase, increasing the amount of Mn(III) species. These results support the XRD analysis. The manganese AOS of the other samples are similar (values between 3.72 and 3.78), due to the presence of Mn(IV) and Mn(III) species (in the case of the Mn5 sample, Mn(IV), Mn(III) and Mn(II)).

3.1.3 BET Surface Area

The BET surface areas of manganese oxides prepared with different pH and template cation are listed in Table 3. As can be seen, the manganese oxide materials have surface areas that range from 25 to 84 m^2/g. However, we must refer that N_2 adsorption at 77 K is not suitable for the characterization of the micropores in this kind of tunnel structured manganese oxides [25]. There is no apparent correlation between the pH and the surface areas obtained. The highest surface area was obtained for the Mn5 sample, which has the cryptomelane structure and small amounts of Mn_3O_4.

3.1.4 Thermal Stability

The thermal stability of manganese oxides was studied by TGA in air and nitrogen atmospheres (Fig. 3) and TPD in a helium atmosphere (Fig. 4). From TGA experiments, it can be seen that for all materials the weight loss under air is lower than in nitrogen atmosphere, due to the reduction of manganese species. Comparing the thermal stability of Mn1, Mn2, Mn3 and Mn4 samples, it seems that the pH used in the synthesis does not affect significantly the TGA profile of the samples (total weight loss ≈ 10–12%). Figure 3 shows that cryptomelane materials have three zones of weight loss under nitrogen. The first occurs at temperatures lower than 200 °C (0.7–1.4%) and is due to the release of water physically adsorbed on the surface of the material, which is consistent with the H_2O profile in TPD (Fig. 4). The amount of water adsorbed is very low, which supports the hydrophobic character of cryptomelane [12]. The second weight loss zone occurs in the range 200–550 °C (1.9–3.4%), and is due to the evolution of chemically adsorbed water and oxygen species from the material (mainly oxygen near the surface) [26]. The last weight loss has been attributed to the evolution of structural oxygen in the framework of the tunnels and occurs in the temperature range 550–900 °C (≈6.7–8.1%). At temperatures higher than 500 °C and under nitrogen atmosphere, the oxygen released from cryptomelane usually leads to the formation of oxygen deficient products such as Mn_2O_3 (≈600 °C) and Mn_3O_4 (≈750–800 °C), and consequently the collapse of the tunnel structure [27]. In summary, the following weight losses were observed: Mn1 (11.4%) > Mn3 (10.9%) > Mn2 (10.3%) > Mn4 (10.0%). These results were expected, since the AOS and the amount of oxygen released are related with each other; justifying the highest and the lowest weight losses observed with Mn1 and Mn4, respectively.

The TGA profiles of the Mn5, Mn6, Mn7 and Mn8 samples are also shown in Fig. 3. The thermal behaviour of Mn5 and Mn6 under nitrogen atmosphere is similar to that of the Mn1–Mn4 samples, although the weight loss is relatively lower (8.1% and 8.5%, respectively) due to the lower average oxidation state. Mn7 and Mn8 also show a smaller weight loss in comparison to Mn1–Mn4, and a gradual weight loss till 700 °C was observed, where all the Mn(III) species are reduced to a lower oxidation state.

The oxygen spectra obtained by TPD are consistent with the TGA results. As can be seen in Fig. 4a, the spectra of Mn1–Mn4 show three peaks: one broad peak in the range 450–550 °C, and two intense and sharp peaks around 600 and 800 °C. Yin et al. [26, 28] have studied the oxygen species in tunnel structured manganese oxides and they suggest that there are three types of oxygen species corresponding to oxygen released in lower temperature regions (LT 250–400 °C), intermediate regions (MT 400–650 °C) and higher temperature regions (HT higher than 650 °C). The α-species (LT peak) was assigned to chemisorbed oxygen species. The β and γ (MT and HT peaks, respectively) species were believed to be due to different structural oxygen species bound to manganese cations: lower manganese valency, and Mn(IV), respectively. Accordingly, it can be seen that in all samples most of the oxygen species can be ascribed to structural oxygen. The evolution of oxygen from the samples prepared at different pH is quite similar, except in the case of lowest pH where the MT peak shifts to lower temperatures. This behaviour indicates that this sample has different Mn–O bond strengths.

Figure 4b shows the TPD spectra of Mn5, Mn6, Mn7 and Mn8. The Mn5 sample shows a small peak at medium

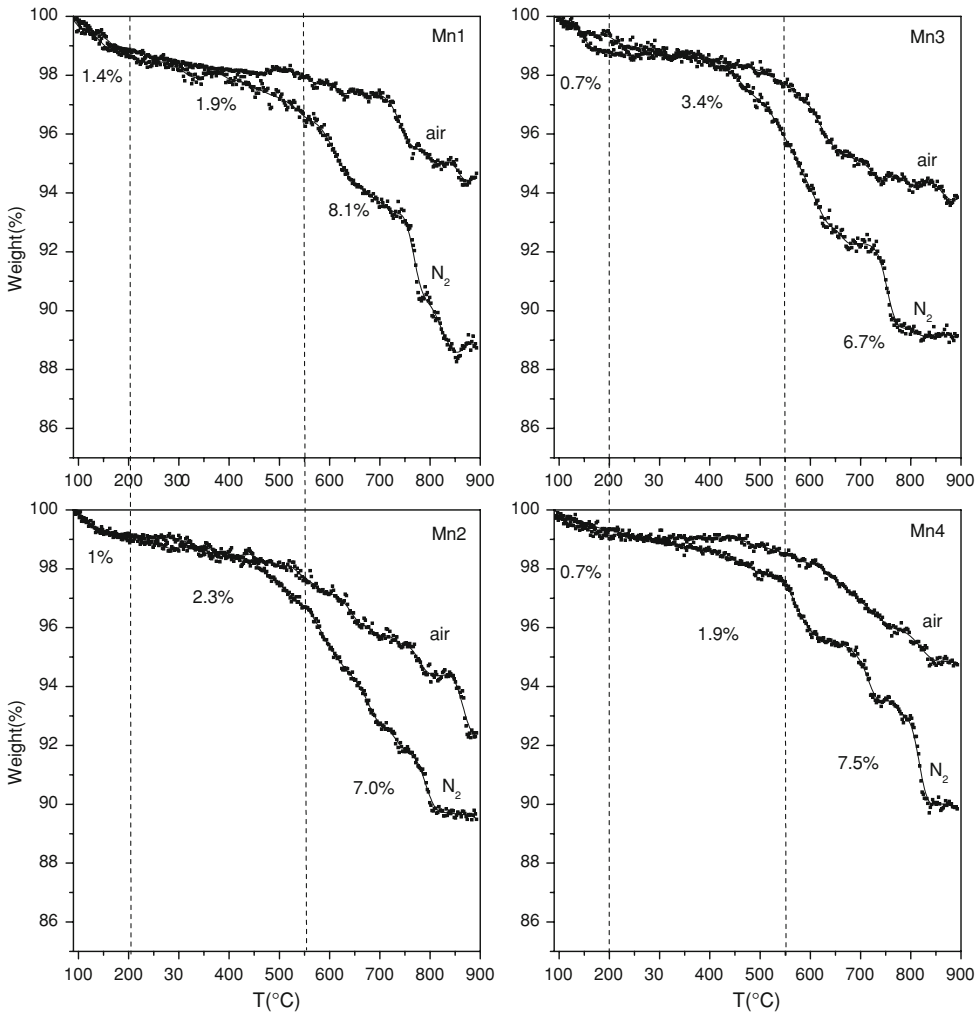

Fig. 3 TGA experiments under nitrogen and air atmospheres. Heating rate: 10 °C/min

temperatures and an intense peak at higher temperatures. The Mn6 sample shows three peaks in the temperature range of 400–900 °C, which indicate three different strengths of Mn–O bonds associated to different manganese valence. Mn7 and Mn8 show only two strong peaks at 525–550 °C and 850 °C, suggesting two different strengths of Mn–O bonds. This is supported by XRD analysis, which shows the presence of Mn(III) and Mn(IV) species.

During TPD analysis, traces of CO_2 have been detected. Two main broad peaks at 250 and 600 °C were observed, suggesting that CO_2 molecules are adsorbed on different sites.

3.2 Catalytic Activity

3.2.1 Screening Tests

The catalytic activities of all materials for the total oxidation of ethyl acetate were evaluated. This study was carried out in order to determine the effect of the physical and chemical properties of the materials, such as structure, surface area and manganese average oxidation state.

The light-off curves of ethyl acetate on the manganese based catalysts are shown in Fig. 5. As can be seen in Fig. 5a and b, no significant change in the catalytic behaviour was observed when the pH used in the preparation was varied from 3.5 to 4.5 and complete oxidation into CO_2 occurs at 215–220 °C. With the Mn3 sample, the catalytic activity is slightly lower at low temperatures (200–215 °C), but complete oxidation to CO_2 occurs at almost the same temperature. The sample prepared at the lowest pH (sample Mn4) presents a significantly lower activity, since the temperature for complete oxidation into CO_2 is approximately 20 °C higher than with the other materials. The main by-product detected in all these experiments is acetaldehyde.

According to these results, it can be stated that the catalytic activity of these materials cannot be correlated with the surfaces areas (Table 3), as Mn1 has practically the same activity as Mn2 and Mn3, in spite of their different surface areas. Therefore, it is probable that the catalytic activity may be related to the structure and the manganese species on the catalyst surface (and consequently with the AOS).

Fig. 3 continued

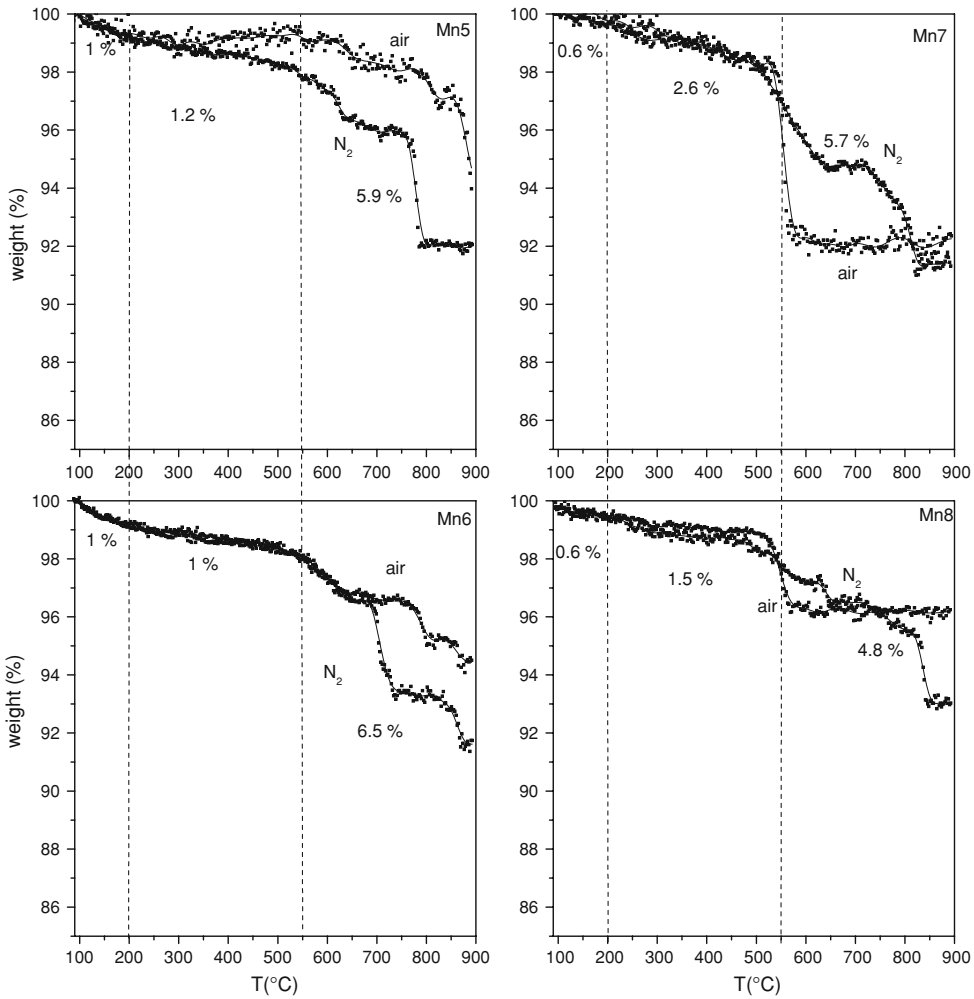

This assumption seems reasonable because it has been suggested that the oxidation of organic molecules with manganese oxide catalysts at low temperatures may involve a Mars and van Krevelen (MVK) mechanism which includes a redox cycle on the catalyst surface with the participation of the lattice oxygen from the oxide [25, 29, 30]. Following the MVK concept, it could thus be predicted that oxides with the highest oxidation state would have the highest oxidation activities, because they have more oxygen atoms that can be used for the VOC oxidation. However, the activity of an oxide is also related to the energy needed to transfer their lattice oxygen atoms to the hydrocarbon, as this energy depends on the global oxidation state of the catalyst. Therefore, the most efficient catalyst for promoting oxidation reactions might not be the fully oxidised one.

It can be observed from Table 3 that AOS and catalytic activities are correlated with each other. Indeed, samples Mn1 and Mn2, with the highest AOS, are the most active, followed by sample Mn3, with a lower AOS. Sample Mn4 has the lowest AOS and is much less active; however, in this case, we do not have a pure cryptomelane phase (Table 2). Xia et al. [31] have also observed that the performances of Cu-OMS-2, Co-OMS-2 and Ag-OMS-2 catalysts for the oxidation of CO were also related to the manganese average oxidation state.

Figure 5c and d show the light-off curves for Mn1, Mn5 and Mn6 samples. The following activity sequence was obtained: Mn5 (100% X_{CO_2} at 215 °C) > Mn1 (100% X_{CO_2} at 220 °C) > Mn6 (100% X_{CO_2} at 240°C). This activity sequence was not expected since the manganese average oxidation state of Mn5 is lower than of Mn1. However, the catalytic performance of the Mn5 sample may be correlated with the presence of small amounts of Mn_3O_4, detected by XRD analysis. Therefore, the presence of the manganese redox pair Mn(II)/Mn(III) in Mn_3O_4 should improve the performance of the catalyst. In fact, the presence of Mn(II) species can make this catalyst more active, as it can exchange oxygen more easily (the Mn(II)–O bond is weaker, which leads to the formation of more active oxygen species) [32]. Chen et al. [33] also observed this catalytic behaviour in the decomposition of 2-propanol over a series of metal doped OMS-2 materials. They observed that during the reaction over Cu-OMS-2 there was a gradual phase transition from cryptomelane to

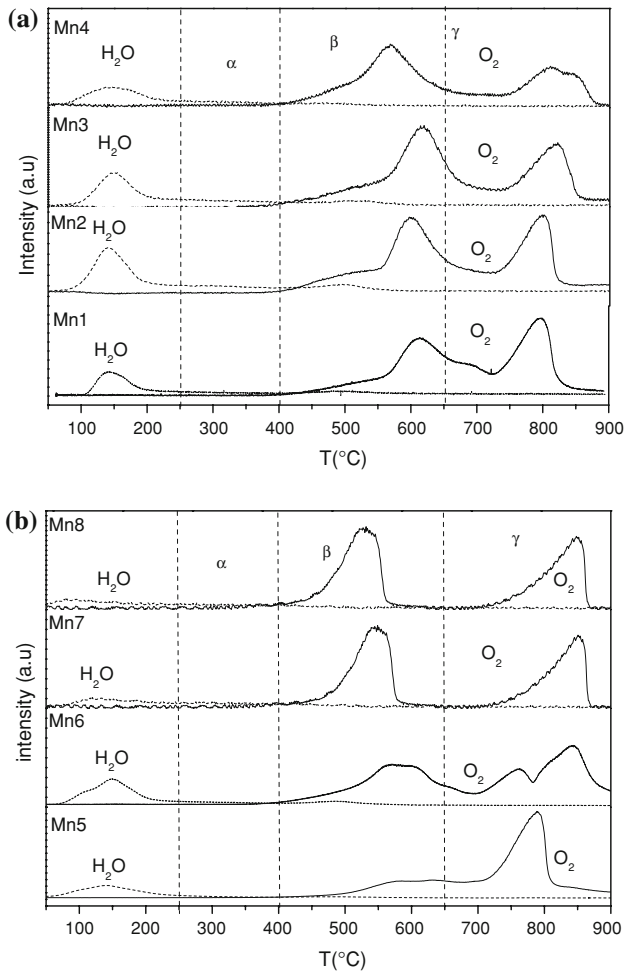

Fig. 4 TPD of O_2 and H_2O of all materials synthesized: **a** Mn1–Mn4, **b** Mn5–Mn8. Heating rate: 5 °C/min

Mn_3O_4, and the presence of the two phases improved the performance of the catalyst.

The manganese oxidation state of the Mn6 sample is quite similar to that of Mn4, and the complete oxidation of ethyl acetate occurs at the same temperature. At low temperatures, this catalyst has an activity a little higher than the Mn4 sample. The catalytic activities of Mn7 and Mn8 are similar to the Mn6 sample, in spite of their different surface areas, promoting the complete oxidation of ethyl acetate into CO_2 at 240 °C (Fig. 5e and f).

These results show that cryptomelane type manganese oxides are very active and selective. The Mn1 sample was selected for further studies.

3.2.2 *Stability Tests*

In order to analyse the stability of the catalyst, long duration experiments were made on the Mn1 sample. The conversion into CO_2 at 210 °C as a function of time on stream (TOS) is shown in Fig. 6. The reaction temperature was selected in order to achieve a high initial ethyl acetate conversion (about 96%). After a period of about 20 h, the conversion reached an almost constant value. The conversion history during the first 2.5 h is similar to those obtained by the light-off curves; the presence of an initial stabilization period has been reported for the catalytic oxidation of ethyl acetate, n-hexane and benzene on γ-MnO_2 [34]. It can be considered that the stabilization period of about 16 h represents the time needed to obtain a constant coverage of the catalyst surface by the reactants and products, especially water [24]. The slight activity decrease which occurs during this period was attributed to a competition of the reactants and water for specific sites [35]. Other authors explain this deactivation by the accumulation of heavy products on the surface, blocking the active sites [36]. In order to understand the activity decay in our system (9.6%), TPO experiments were made after stopping the reaction at different TOS. The total amount of coke does not increase with TOS, its value being very low (0.05 wt%), as can be seen in Table 4. In order to confirm this result, another stability test was made at lower temperature (180 °C), and TPO experiments were carried out after 1 and 20 h of the reaction. Similar results were obtained (Table 4), i.e, coke does not accumulate on the catalyst.

3.2.3 *Influence of Water Vapour or CO_2 in the Feed Stream*

The performance of catalyst Mn1 was also tested in the standard conditions (16,000 h^{-1}, 1600 ppmv) with water vapour or CO_2 added to the inlet stream. In industrial applications, humidity and CO_2 will be present in the effluents to be treated, so it is important to know the performance of cryptomelane in these conditions. Therefore, 2% of water vapour or 2% of CO_2 were individually introduced in the feed. The light-off curves are compared in Fig. 7. In the presence of 2% of H_2O, there is no significant difference in the temperature for total oxidation of ethyl acetate, but at lower temperatures slightly lower conversions were observed. This behaviour is quite different from supported platinum catalysts (namely Pt/TiO_2), where the presence of water vapour increases the global conversion but decreases the CO_2 yield [34]. At 210 °C, the conversion into CO_2 changes from 0.85 to 0.65 in the presence of water vapour. Nevertheless, this catalyst can still oxidise completely ethyl acetate into CO_2 at the same temperature of 220 °C. In order to understand this behaviour, TPO experiments were conducted at 180 °C in the presence and in the absence of water vapour. It was observed that there were no significant differences in the coke content. In addition to the results described above, the behaviour of

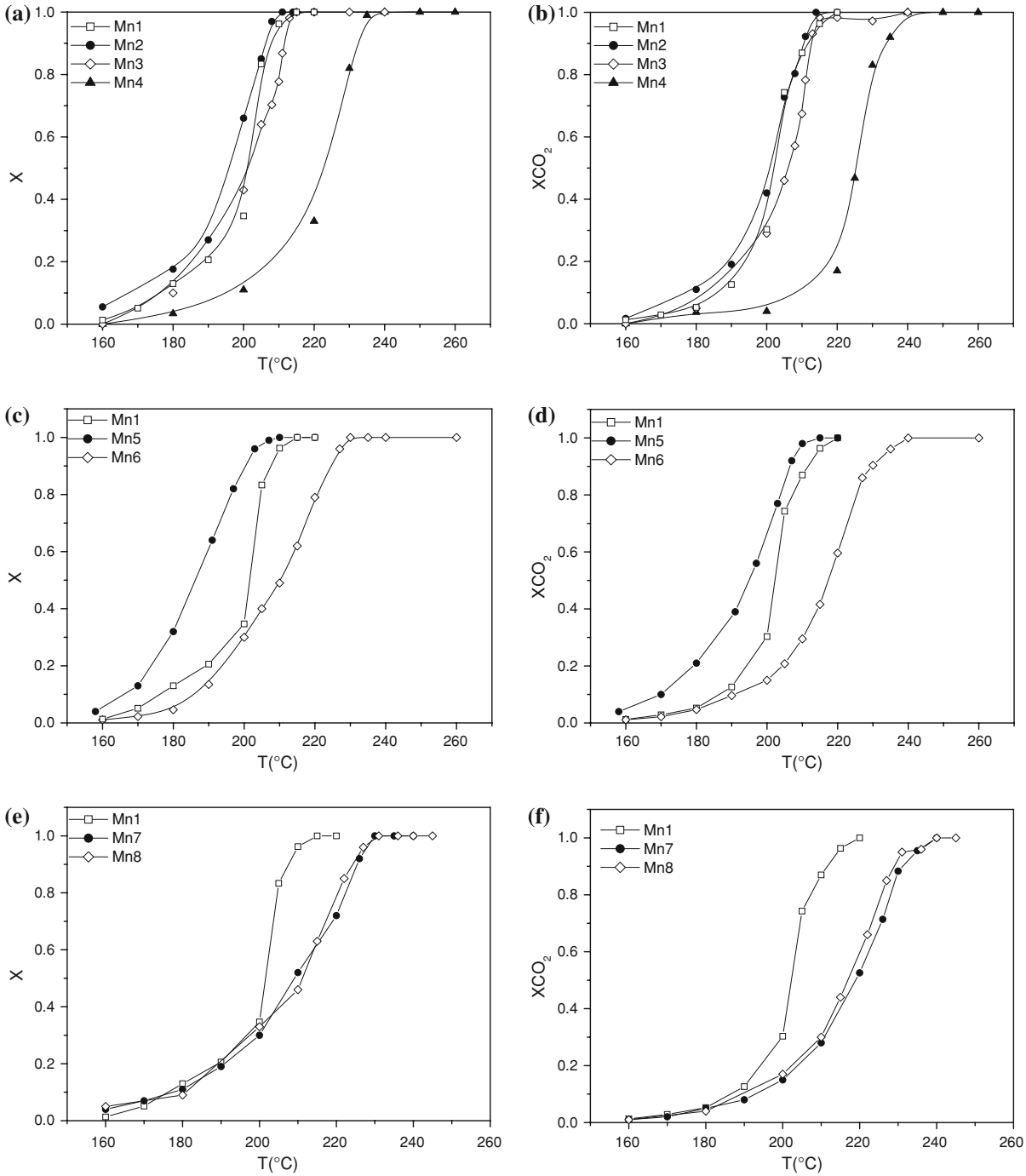

Fig. 5 Performance of manganese oxide catalysts on the total oxidation of ethyl acetate (space velocity: 16,000 h^{-1}, inlet VOC concentration: 1,600 ppmv)

catalyst Mn1 in the presence of 2% CO_2 was also investigated. As can be seen in Fig. 7, no significant effect was observed when CO_2 was present, in the temperature range studied. This behaviour shows that there is no competition between the reactants and CO_2 for the active sites involved in the reaction mechanism.

4 Conclusions

Cryptomelane type manganese oxide was synthesized using a reflux method. The synthesis parameters studied were the acidity of the solution and the template cation. The following conclusions can be drawn:

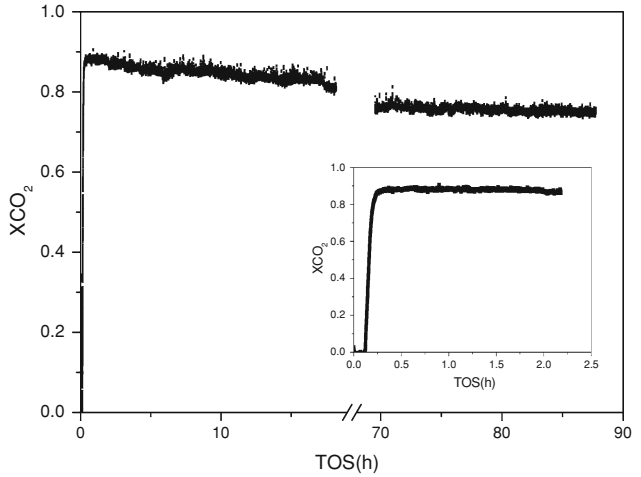

Fig. 6 Evolution of the conversion into CO_2 with time on stream on the Mn1 sample at 210 °C

Table 4 Amount of coke on the Mn1 sample as a function of time on stream (TOS)

Temperature (°C)	TOS (h)	g C/100 gcat
210	1	0.05
210	90	0.05
180	1	0.27
180	20	0.29

1. At very low pH (pH 2) no pure cryptomelane phase was obtained, but instead a mixture of α-Mn_2O_3 and cryptomelane. In the pH range 4.5–3.0 a pure cryptomelane phase was produced, and there are no significant differences between the use of buffer solution or nitric acid for pH control, except in the fibers width.
2. During the reflux treatment the presence of potassium cations is necessary to support and stabilize the tunnel structure of cryptomelane. When no source of potassium cations was used in the reactant mixture, no cryptomelane phase was obtained, but instead a mixture of β-MnO_2 and α-Mn_2O_3. The morphology of the materials depends on the source of permanganate.
3. All the manganese oxides synthesised in this study were active for the total oxidation of ethyl acetate into CO_2. All the catalysts oxidize ethyl acetate into CO_2 at temperatures below 250 °C.
4. The activity of the catalysts seems to be correlated mainly with the average oxidation state of the manganese oxides.
5. The highest activity was obtained for the cryptomelane-type manganese oxide catalyst. Small amounts of Mn_3O_4 increase the performance of this catalyst.
6. Long duration experiments show that there is a slight deactivation of the catalyst in the first 20 h of reaction, being stable afterwards. This deactivation is not due to the accumulation of coke.
7. The presence of water vapour and CO_2 in the feed does not have a major influence on the performance of cryptomelane for the total oxidation of ethyl acetate, although the catalytic performance is slightly affected at low temperatures in the presence of water vapour.

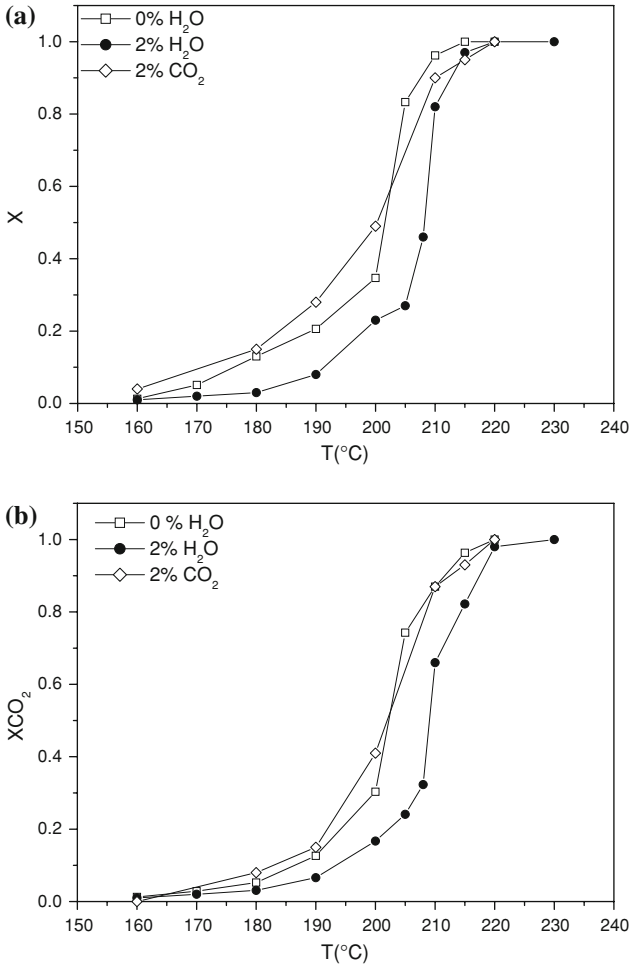

Fig. 7 Influence of water vapour or CO_2 on the performance of the cryptomelane catalyst (Mn1 sample): **a** ethyl acetate conversion, **b** conversion into CO_2

Acknowledgments This work was supported by Fundação para a Ciência e a Tecnologia (FCT) and FEDER under Programme POCTI/1181 and PTDC/AMB/69065/2006. V·P.S. acknowledges the grant received from FCT (SFRH/BD/23731/2005). The authors also acknowledge the Programme CYTED (PI0269) and Dr. Carlos M. Sá (CEMUP) for assistance with XPS analyses.

References

1. Post JE (1999) Proc Natl Acad Sci U S A 96:3447
2. Suib SL (1998) Curr Opin Solid State Mater Sci 3:63

3. Brock SL, Duan NG, Tian ZR, Giraldo O, Zhou H, Suib SL (1998) Chem Mater 10:2619
4. Shen YF, Zerger RP, Deguzman RN, Suib SL, McCurdy L, Potter DI, Oyoung CL (1993) Science 260:511
5. Frias D, Nousir S, Barrio I, Montes M, Lopez T, Centeno MA, Odriozola JA (2007) Mater Charact 58:776
6. DeGuzman RN, Shen YF, Neth EJ, Suib SL, Oyoung CL, Levine S, Newsam JM (1994) Chem Mater 6:815
7. Villegas JC, Garces LJ, Gomez S, Durand JP, Suib SL (2005) Chem Mater 17:1910
8. Ching S, Suib SL (1997) Comments Inorg Chem 9:263
9. Lamaita L, Peluso MA, Sambeth JE, Thomas HJ (2005) Appl Catal B-Environ 61:114
10. Parida KM, Samal A (1999) Appl Catal A-Gen 182:249
11. Liu J, Makwana V, Cai J, Suib SL, Aindow M (2003) J Phys Chem B 107:9185
12. Suib SL (2008) J Mater Chem 18:1623
13. Feng Q, Kanoh H, Ooi K (1999) J Mater Chem 9:319
14. Feng Q, Yanagisawa K, Yamasaki N (1998) J Porous Mater 5:153
15. Luo J, Zhang Q, Huang A, Suib SL (2000) Microporous Mesoporous Mater 35–36:209
16. Malinger KA, Ding YS, Sithambaram S, Espinal L, Gomez S, Suib SL (2006) J Catal 239:290
17. Ching S, Roark JL, Duan N, Suib SL (1997) Chem Mater 9:750
18. Welch E, Bahadoor A, Hughes S, Ching S (2001) Am Chem Soc 221:U159 Abstract Paper
19. Ding YS, Shen XF, Sithambaram S, Gomez S, Kumar R, Crisostomo VMB, Suib SL, Aindow M (2005) Chem Mater 17:5382
20. Shen YF, Zerger RP, Suib SL, McCurdy L, Potter DI, Oyoung CL (1992) J Chem Soc Chem Commun 1213
21. Yang LX, Zhu YJ, Wang WW, Tong H, Ruan ML (2006) J Phys Chem B 110:6609
22. Rojas ML, Fierro JLG, Tejuca LG, Bell AT (1990) J Catal 124:41
23. Galakhov VR, Demeter M, Bartkowski S, Neumann M, Ovechkina NA, Kurmaev EZ, Logachevskaya NI, Mukovskii YM, Mitchell J, Ederer DL (2002) Phys Rev B 65:4
24. Wang X, Cui QL, Pan YW, Zou GT (2003) J Alloy Compd 354:91
25. Luo J, Zhang Q, Garcia-Martinez J, Suib SL (2008) J Am Chem Soc 130:3198
26. Yin YG, Xu WQ, Shen YF, Suib SL, Oyoung CL (1994) Chem Mater 6:1803
27. Bish DL, Post JE (1989) Am Miner 74:177
28. Yin YG, Xu WQ, Suib SL, Oyoung CL (1995) Inorg Chem 34:4187
29. Baldi M, Finocchio E, Milella F, Busca G (1998) Appl Catal B-Environ 16:43
30. Cellier C, Ruaux V, Lahousse C, Grange P, Gaigneaux EM (2006) Catal Today 117:350
31. Xia GG, Yin YG, Willis WS, Wang JY, Suib SL (1999) J Catal 185:91
32. Peluso MA, Gambaro LA, Pronsato E, Gazzoli D, Thomas HJ, Sambeth JE (2008) Catal Today 133–135:487
33. Chen X, Shen YF, Suib SL, O'Young CL (2001) J Catal 197:292
34. Lahousse C, Bernier A, Grange P, Delmon B, Papaefthimiou P, Ioannides T, Verykios X (1998) J Catal 178:214
35. Gandia LM, Gil A, Korili SA (2001) Appl Catal B-Environ 33:1
36. Paulis M, Gandia LM, Gil A, Sambeth J, Odriozola JA, Montes M (2000) Appl Catal B-Environ 26:37